European Journal of Medicinal Chemistry 46 (2011) 5949–5958

Contents lists available at SciVerse ScienceDirect

European Journal of Medicinal Chemistry

journal homepage: http://www.elsevier.com/locate/ejmech

Original article

Pharmacophore identification, virtual screening and biological evaluation of prenylated flavonoids derivatives as PKB/Akt1 inhibitors

Xiaowu Dong [a], Xinglu Zhou [b], Hui Jing [b], Jianzhong Chen [a], Tao Liu [a], Bo Yang [b], Qiaojun He [b], Yongzhou Hu [a,*]

[a] ZJU-ENS Joint Laboratory of Medicinal Chemistry, College of Pharmaceutical Sciences, Zhejiang University, Hangzhou 310058, China
[b] Institute of Pharmacology & Toxicology, College of Pharmaceutical Sciences, Zhejiang University, Hangzhou 310058, China

ARTICLE INFO

Article history:
Received 14 May 2011
Received in revised form
25 September 2011
Accepted 2 October 2011
Available online 8 October 2011

Keywords:
PKB/Akt1
Pharmacophore model
HypoGen
Molecular docking
Virtual screening

ABSTRACT

A total of 24 well-defined PKB/Akt1 inhibitors were used to generate pharmacophore models applying Catalyst/HypoGen program. The best ranked model (Hypo_1) was then validated by cost analysis, prediction capability, Cat-Scramble and receiver operating characteristic (ROC) studies. Then, pharmacophore-based virtual screening combined with docking study was performed to search an in-house compound database. Nine preferable hits **75**–**80**, **HTS-02143**, **BTB-14740** and **HTS-08006** were prepared and biologically evaluated. Several compounds were identified as good PKB/Akt1 inhibitors, suggesting that Hypo_1 would be reliable and useful in virtual screening. Flow cytometric and western blotting analysis on compounds **79** and **80** further demonstrated that the inhibition of phosphorylation of PKB/Akt1 and its substrates (such as GSK3β) was responsible for their cytotoxic activities.

1. Introduction

PKB/Akt, the serine/threonine proteases, belongs to the AGC family of kinases. It is a central node of the PI3K/Akt signaling pathway which is one of the most frequently mutated or over expressed signaling abnormality in cancers [1–4]. PKB/Akt can be classified into three subfamilies: PKB/Akt1, PKB/Akt2 and PKB/Akt3 [5]. PKB/Akt have a high degree of overall homology being approximately 80% identical [6], and share similar downstream targets, but differ in the levels of expression and activation in various tumors [7]. Inhibition of PKB/Akt alone or in combination with other cancer chemotherapeutics can result in increasing apoptosis of cancer cells, decreasing tumor growth and reversing tumor resistance [8–10]. All of these findings led to extensive studies of PKB/Akt inhibitors as anticancer agents. In general, there are three strategies applied to development of novel PKB/Akt inhibitors, targeting toward pleckstrin homology (PH) domain [11], ATP-binding kinase domain [12], and hinge-region domain [13]. Among these approaches, the most highly explored strategy is to target ATP-binding kinase domain, leading to discover lots of potent PKB/Akt inhibitors, such as bis-pyridinylethylenes [14], isoquinoline (indazole)–pyridines [15,16], pyridine–pyrazolopyridine [17] and oxindole–pyridine [18]. However, drawbacks of this kind of inhibitors as a clinical agent lie in their short half-life in animals and poor oral bioavailability [17]. Therefore, it is still greatly interested and valued in searching novel chemical scaffolds with PKB/Akt inhibitory activity.

Pharmacophore-based virtual screening is a rational strategy for identification of novel hits or leads with diverse chemical scaffolds [19,20]. There are several methods for generation of pharmacophore models, such as HypoGen [21], MOE [22], Phase [23] and GALAHAD [24]. HypoGen is one of the most widely used approaches in pharmacophore-based drug design. Böhm *et al.* identified several DNA gyrase inhibitors with novel scaffolds using Catalyst and LUDI programs to screen Available Chemical Dictionary (ACD) and Roche compound inventory (RCI) database [25]. Besides, Catalyst/HypoGen was applied by Yu *et al.* to establish a pharmacophore model of KDR kinase inhibitors and successfully discovered a novel hit in screening the Traditional Chinese Medicine Database (TCMD) [26]. Nevertheless, few reports about pharmacophore-based virtual screening for discovering novel PKB/Akt inhibitors are available.

In the present study, a novel pharmacophore model was proposed based on a set of pyridinyl-bridged PKB/Akt1 inhibitors using Catalyst/HypoGen program (Catalyst 4.1, Molecular Simulations Inc., San Diego, CA). The pharmacophoric features in Hypo_1 was then demonstrated to be consistent with the interaction mode

* Corresponding author. Tel./fax: +86 571 888208460.
E-mail addresses: huyz@zju.edu.cn, huyz@zjuem.zju.edu.cn (Y. Hu).

0223-5234/$ – see front matter © 2011 Elsevier Masson SAS. All rights reserved.
doi:10.1016/j.ejmech.2011.10.006

proposed in molecular docking, which was carried out to evaluate the molecular interactions between the hits and PKB/Akt1. Finally, the preferably screened hits were picked up and biologically evaluated to validate robustness and predictive ability of the virtual screening model.

2. Computational methods

2.1. Generation of pharmacophore models

For the pharmacophore modeling studies, a set of 74 compounds were selected from the literatures [14–16,27]. PKB/Akt1 inhibitory activity data (IC_{50}, Table 1) of them span over 6 orders of magnitude (from 0.16 to 32250 nM). The 2D structures of these compounds were illustrated in Fig. 1. The dataset was split into a training set of 24 compounds and a test set of 50 compounds. Besides, the 1940 negatives compounds used in receiver operating characteristic (ROC) were retrieved from Available Chemical Directory (ACD) database (Symyx Technologies, Santa Clara, CA) using "Random Percent Filter protocol" by Pipeline Pilot software (SciTegic, Inc., San Diego, CA). All the compounds were optimized in Discovery Studio 2.0 software (Accelrys, Inc. San Diego, CA) using the CHARMm-like force field [28]. Then, a representative family of conformations was generated for each compound using the Poling Algorithm [29] and the 'best conformational analysis' method with the default parameters in the Catalyst molecular modeling package (Catalyst 4.10 documentation).

An initial analysis of the "show function mapping" tools indicated that five kinds of chemical features, including H-bond acceptor (HBA), H-bond donor (HBD), hydrophobic (HY), aromatic (RA) and positive ionizable (NI) features, effectively map all critical pharmacophoric features of all molecules in both training and test sets. Based on all of these features of 24 compounds in the training set, 10 pharmacophore models were generated using Catalyst/HypoGen program (Catalyst 4.1, Molecular Simulations Inc., San Diego, CA) with the default uncertainty value of 3.0. The uncertainty value represents a ratio range of uncertainty in the activity value based on the expected statistical irregularities of biological data collection.

Table 1
The experimental data and Hypo_1-predicted IC_{50} values of compounds **1**–**74**.

Cmpd.	PKB/Akt1 IC_{50}(nM)		Error factor	Cmpd.	PKB/Akt1 IC_{50}(nM)		Error factor
	Exp.	Pred.			Exp.	Pred.	
1[a,b]	0.16	0.42	2.6	**38**[a]	14170	2800	−5.1
2[a,b]	1.8	5.6	3.1	**39**	5290	8200	1.5
3[a,b]	2.9	13	4.6	**40**	4040	1800	−2.2
4[a,b]	2.6	0.91	−2.9	**41**	6760	760	−8.8
5[b]	1.5	5.5	3.7	**42**	8020	1400	−5.7
6[b]	3.9	10	2.6	**43**	4040	1800	−2.2
7[b]	18	34	1.9	**44**	875	690	−1.3
8[a,b]	13.3	7.6	−1.7	**45**[a]	488	310	−1.6
9[a,b]	18	38	2.1	**46**[a]	312	660	2.1
10	3.6	6.2	1.7	**47**[a]	473	440	−1.1
11	49	4	−12	**48**[a]	685	490	−1.4
12	39	7.6	−5.1	**49**	237	1600	6.8
13[b]	13	1.2	−11	**50**	1232	190	−6.6
14[b]	7.7	8.6	1.1	**51**[b]	92	230	2.5
15	57	13	−4.4	**52**	1117	430	−2.6
16[b]	12.1	10	−1.2	**53**	215	540	2.5
17	3.3	2	−1.6	**54**	1659	540	−3.1
18	126	210	1.7	**55**	4022	410	−9.8
19[b]	14	49	3.5	**56**[a]	1503	590	−2.5
20[b]	6.8	1.4	−4.9	**57**	331	940	2.8
21[b]	78	52	−1.5	**58**	147	20	−7.5
22[a,b]	3.2	7.4	2.3	**59**[b]	7.4	12	1.6
23[a,b]	180	310	1.8	**60**[a]	223	1200	5.3
24	1020	430	−2.4	**61**	760	1100	1.5
25[b]	52.7	600	11	**62**[b]	59	60	1.0
26[a]	121	320	2.7	**63**[a]	13	95	7.3
27[a]	2670	630	−4.2	**64**[b]	6.1	50	8.3
28[a]	953	270	−3.6	**65**	360	1000	2.8
29	6450	570	−11	**66**[b]	28	290	10
30	6350	350	−18	**67**	278	1100	4.1
31	176	88	−2.0	**68**	3200	6400	2.0
32	147	580	3.9	**69**	668	2400	3.6
33	3340	850	−3.9	**70**	300	1200	−0.6
34[a]	23910	62000	2.6	**71**[a]	1100	400	−2.8
35[a]	32250	5500	−5.9	**72**[a]	23270	5200	−4.5
36[a]	146	560	3.9	**73**	190	980	−0.71
37[a]	5080	2300	−2.2	**74**	198	380	1.9

[a] The compounds were used as test set.
[b] The compounds were used as active compounds (positive) in ROC studies.

2.2. Pharmacophore model quality examination

In order to evaluate the reliability and accuracy of the generated 3D pharmacophore models, cost analysis, prediction capability, Cat-Scramble validation and receiver operating characteristic (ROC) studies were performed.

2.2.1. Cost analysis

The quality of HypoGen-generated pharmacophore models can be described in terms of fixed cost, null cost and total cost, all of which are well-defined by Debnath [30]. The fixed cost represents the simplest model that fits the data. The null cost represents the cost of a hypothesis with no features which estimates every activity to be the average activity. If a returned cost (total cost) differs from the null cost by 40–60 bits, it is highly probable that the hypothesis has 75–90% chance representing the true correlation of the data. If the difference becomes more than 60 bits, the probability of representing the true correlation of the data are even higher.

2.2.2. Prediction capability of the generated pharmacophore model

The pharmacophore model was also used to predict the PKB/Akt inhibitory activities of other compounds beyond in the training set. For such a purpose, 50 PKB/Akt1 inhibitors in the test set were estimated by the best pharmacophore model which has the highest correlation coefficient (r), lowest total cost, and lowest RMSD value.

2.2.3. Cat-Scramble validation

The Cat-Scramble validation procedure is based on Fischer's randomization test [31]. It is to check whether there is a strong correlation between chemical structures and bioactivities of ligands. It is done by randomizing the activity data associated with the training set of compounds and by generating pharmacophore hypotheses using the common chemical features and parameters to develop the original pharmacophore hypothesis. 19 random spreadsheets are generated for 95% confidence level. If the randomized data set has the similar or better cost values, RMSD and correlation in the generation of a pharmacophore model, the original hypothesis is considered to have been generated by chance.

2.2.4. Receiver operating characteristic (ROC) studies

An in-house database was retrieved randomly from Available Chemicals Directory (ACD) database (1940 molecues) spiked some known PKB/Akt1 inhibitors (24 molecues, Table 1). The receiver operating characteristic (ROC) study using the Hypo_1 to screen this in-house database were further performed [32]. True positive rate (TPR) and false positive rate (FPR) from a comparison between *in vitro* and *in silico* activities were calculated.

$$\mathrm{TPR} = \frac{\mathrm{TP}}{\mathrm{TP} + \mathrm{FN}}$$

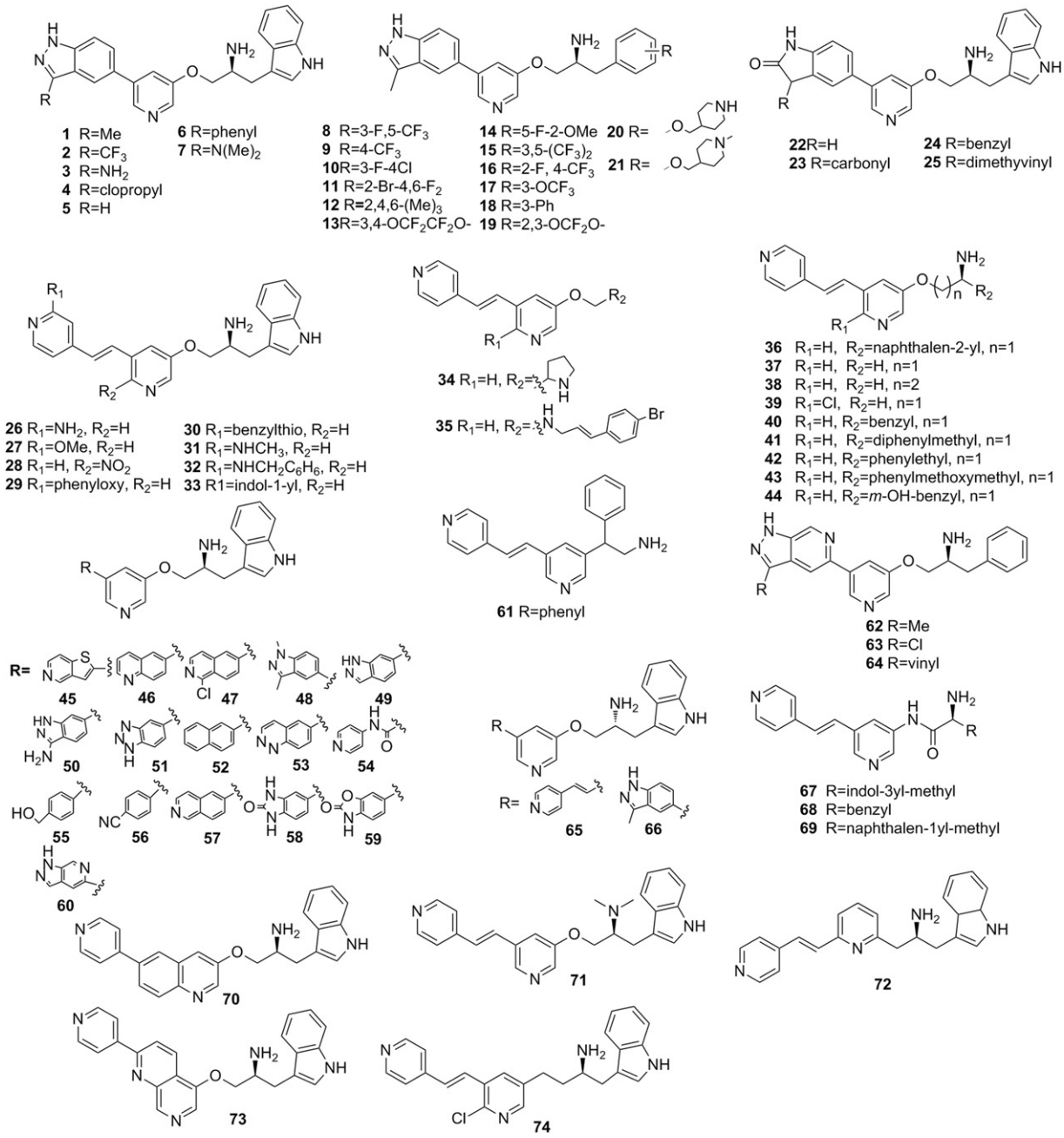

Fig. 1. The 2D structures of 74 PKB/Akt1 inhibitors used to generate the pharmacophore model.

where TP is the number of true positive compounds, FN is the number of false negative compounds.

$$\mathrm{FPR} = \frac{\mathrm{FP}}{\mathrm{TN} + \mathrm{FP}}$$

where TN is the number of true negative compounds, FP is the number of false positive compounds.

The ROC curve is a function of FPR versus the TPR, and the area under the ROC curve (AUC) value is the important way of measuring the performance of the test.

$$\mathrm{AUC} = \sum_{x=2}^{N} \mathrm{TPR}(x)[\mathrm{FPR}(x) - \mathrm{FPR}(x-1)]$$

where TPR(x) is the percent of the true positives versus the total positives at rank position x, FPR(x) is the percent of the false positives versus the total negatives at rank position x.

2.3. Molecular docking with FlexiDock program

The X-ray crystal structure of PKB/Akt1 (PDB code: 3COB) was retrieved from the Protein Data Bank (PDB, http://www.pdb.org). ATP competitive binding pocket was defined to cover all residues within 4 Å of the ligand in the crystal PKB/Akt1-ligand complex. All single bonds of residue side chains inside the defined binding pocket were regarded as flexible. The compounds were allowed to rotate on all of single bonds and move flexibly within the tentative

binding pocket. The atomic charges were recalculated using the Kollman all-atom approach for the protein.

3. Results and discussion

3.1. HypoGen-generated pharmacophore models

Table 2 displays a set of 10 pharmacophore hypotheses generated from the training set of 24 PKB/Akt1 inhibitors using Catalyst/HypoGen. Among these 10 hypotheses, Hypo_1 is characterized by the highest cost difference of 75.68, the lowest RMSD of 0.987, and the highest correlation coefficient of 0.948. Noticeably, the cost range between Hypo_1 and the fixed cost is 17.03, while that between the null hypothesis and Hypo_1 is 75.68, showing that Hypo_1 has more than 90% probability of correlating the data. Fig. 2A shows the topological features of Hypo_1 which consists of four pharmacophore features, including one H-bond acceptor (HBA, colored by green), two H-bond donors (HBD, colored by purple), and one hydrophobic group (HY, colored by cyan).

The predicted results of PKB/Akt inhibitory activities (IC_{50} values) of the 24 training set molecules are listed in Table 1, and the plots of predicted versus experimental values are recorded in Fig. 2B. It is demonstrated that the activities of most compounds are predicted correctly. For example, as shown in Fig. 2A, the superimposition of Hypo_1 with the most active compound **1** (IC_{50} = 0.16 nM) indicated that all Hypo_1's features of HBA, HBD, and HY are mapped very well onto the compound **1** (prediction IC_{50}: 0.41 nM; actual IC_{50}: 0.16 nM). In the case of **34**, the HBD1 and HBA features cannot fit well to the corresponding pharmacophore features while the HBD2 feature is missed (Fig. 2A), leading to a poor predicted activity but close to its actual activity (prediction IC_{50}: 62,000 nM; actual IC_{50}: 23,910 nM).

3.2. Prediction capability of the generated pharmacophore model

3.2.1. Test set prediction

In order to verify whether Hypo_1 can also predict the activities of compounds beyond the training set, we applied a total of 50 compounds representing diverse activity classes and different structural groups as test set. As shown in Fig. 2B, there is a good line correlation between the experimental and predicted PKB/akt1 activities of the test set compounds, showing a good correlation coefficient of 0.803. Thus, Hypo_1 has a good prediction capability for both training set and test set compounds.

3.2.2. Cat-Scramble validation

With the aid of the Cat-Scramble program, the experimental activities of compounds in the training set were scrambled randomly, and the resulting data set were used for HypoGen generation. All parameters were adopted and used in the initial HypoGen calculation. This procedure was reiterated 19 times. As shown in Fig. 2C, none of the outcome hypotheses has a lower cost score than the initial hypothesis (Hypo_1), suggesting that there is a strong correlation between chemical structures and biological activities for Hypo_1 and it is not generated by chance.

Table 2
Information of statistical significance and predictive power presented in cost values measured for top 10 hypotheses as a result of HypoGen generation process.

Hypo. no.	Total cost	Δcost	RMSD	Correl.
1	111.47	75.68	0.987	0.948
2	117.23	69.92	1.275	0.906
3	118.10	69.05	1.288	0.904
4	112.77	74.38	1.514	0.861
5	123.02	64.13	1.507	0.863
6	123.72	63.43	1.415	0.884
7	124.86	62.29	1.489	0.869
8	125.48	61.67	1.598	0.843
9	125.61	61.54	1.577	0.849
10	125.99	61.16	1.597	0.845

Null cost of 10 top-scored hypotheses is 187.15, fixed cost value is 94.43 and configuration cost is 12.59.

3.2.3. Receiver operating characteristic (ROC) studies

The Hypo_1 was further validated for picking up PKB/akt1 inhibitors from a database, including 1940 inactive compounds and 24 known PKB/akt1 inhibitors (labeled in Table 1). The ROC curves (Fig. 2D) was obtained with good AUC value of 0.957, which was equal to the probability that a classifier will rank a randomly chosen positive instance much higher than a randomly chosen negative one. Hypo_1 is a useful and reliable tool for identifying novel PKB/Akt inhibitors in virtual screen.

3.3. Interaction mode between PKB/Akt1 and ligands proposed by molecular docking

Although a number of sophisticated techniques are available to benchmark docking success rate, one particular method has been the most widely used where one defines the successfully docked ligand as a top-scored pose with small RMSD value from the reference coordinates. Herein, we compared with the re-docking results using FlexiDock [33], FlexX [34], LigandFit [35], CDOCKER [36] and Libdock [37] base on six PKB/Akt1−ligand complex (PDB code: 3CQU, 3CQW, 3MV5, 3MVH, 3OCB and 3OW4) that was retrieved from the Protein Data Bank (PDB, http://www.pdb.org). Each RMSD value of proposed ligands from the reference coordinates was recorded, and the average RMSD value was calculated as the evaluation criteria for selection of the most preferable docking program. As shown in Fig. 3a, it is obvious that FlexiDock is the best program for studying the interaction mode between PKB/Akt1 and ligands (average RMSD is 0.44).

Furthermore, the interaction between compound **1** and PKB/Akt1 (PDB entry code: 3OCB) was studied using FlexiDock program. The simulated model of compound **1**-PKB/Akt1 complex is depicted in Fig. 3b, showing hydrophobic and hydrogen bond interaction between the ligand and protein. Two H-bonds are formed between indazole moiety of compound **1** and Glu228 and Ala 230 of PKB/Akt1 with a distance of 2.13 Å and 1.43 Å, respectively. 2-NH_2 group in compound **1** can form H-bonds with Asp292 of PKB/Akt1 with a distance of 2.58 Å. In the fourth H-bond formed between ligand and protein, compound **1** provides H-bond acceptor nitrogen atom in pyridinyl ring to form H-bond interaction with Lys179 of PKB/Akt1 with the H-bond length of 1.63 Å. In addition, the aromatic stack interaction between the indole ring of compound **1** and Phe161 of PKB/Akt1 serves to increase the thermal stability of the complex. Such an interactions mapping is consistent with our previous discussion about Hypo_1, in which there are four chemical features, including one HBA, two HBD, and one HY, playing critical roles in the interaction between PKB/Akt1 and ligand.

3.4. Database screening for novel PKB/Akt1 inhibitors

Hypo_l was employed as a 3D search query to screen the in-house database consisting of the compounds synthesized in our lab (1024 molecules) and from Maybridge database (~60,000 molecules). Over 80 hits fitted well with features of Hypo_1 were predicted as potential candidates for further exploration. Considering that pharmacophore mapping and molecular docking complement each other and can be synergistically integrated to

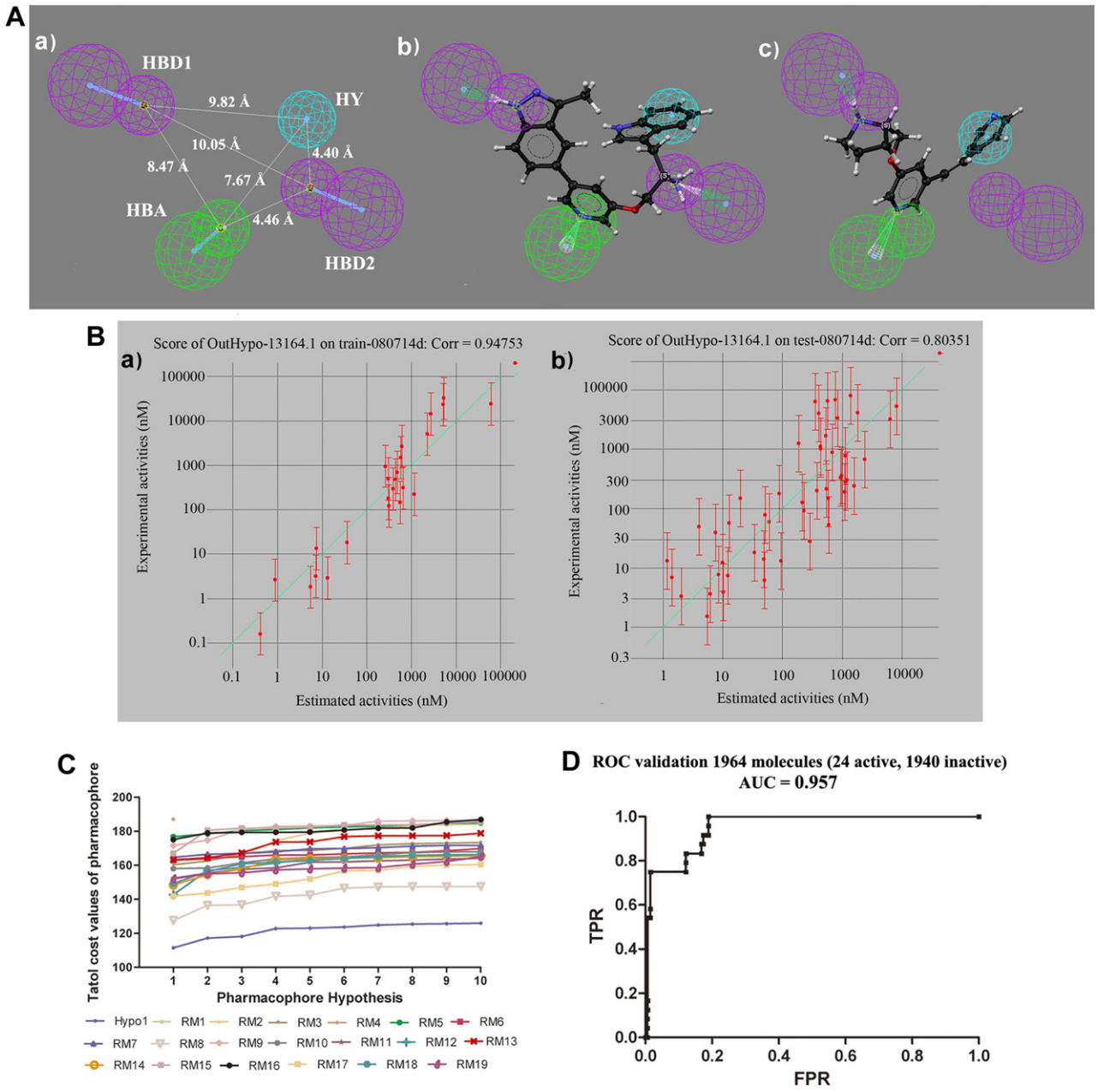

Fig. 2. Hypo_1 was established and validated by cost analysis, prediction capability, Cat-Scramble and receiver operating characteristic (ROC) studies. (A) Hypo_1 and its alignment to representative compounds. The topological features of Hypo_1: four pharmacophoric features, including one hydrophobic group (Cyan), one H-bond acceptor (Green), and two H-bond donors (Purple) (a); Hypo_1 aligned to compound **1** (b); Hypo_1 aligned to compound **37** (c); (B) the prediction ability of Hypo_1. The regression of actual versus predicted activities by the Hypo_1 for training set (a); the regression of actual versus predicted activities by the Hypo_1 for test set inhibitors (b); (C) the difference in costs between the HypoGen runs (Hypo_1) and the scrambled runs (RM1 ~ RM19); (D) ROC curves of the database screening Hypo_1. (For interpretation of the references to colour in this figure legend, the reader is referred to the web version of this article.)

improve the drug design and development process, thus, all the hits obtained by Hypo_1 were further evaluated by docking studies to check their shape fits in the binding site of protein using FlexiDock. Finally, a total of nine preferable compounds **75**–**80**, **HTS-02143**, **BTB-14740** and **HTS-08006** (Fig. 4) were identified as preferable hits in both Hypo_1-based screening and molecular docking studies, the screening results of which are listed in Table 3. In case of compounds **79** and **80**, both of them showed good Fit-value (**79**: 10.8 and **80**: 10.4) and low docking energy (**79**: −3545.0 kal/mol and **80**: −3766.5 kal/mol) in virtual evaluation, leading to a good predicted activity for them. As shown in Fig. 5a,b, 7-hydroxyl and 3′-hydroxyl of **79** (or 7-hydroxyl and 4′-hydroxyl of **80**) were mapped well on HBD_1 and HBD_2 of Hypo_1, while 4-carbonyl and C-6 prenyl of **79** (or 4-carbonyl and C-8 prenyl of **80**) were mapped well on the HBA and HY features of Hypo_1. As shown in Fig. 5c,d, three hydrogen bond interactions are formed between PKB/Akt1 (Lys179, Glu228 and Ala230) and 3′,4′-dihydroxyl and 4-carbonyl groups of **79** (or **80**). In addition, the hydrophobic interaction is observed between C-6 prenyl group of **79** and phenyl group of Phe161, and between C-8 prenyl group of **80** and phenyl group of Phe479.

3.5. Chemistry

In order to validate the reliability of a combination of Hypo_1 and docking studies, all the hits were selected for further studies,

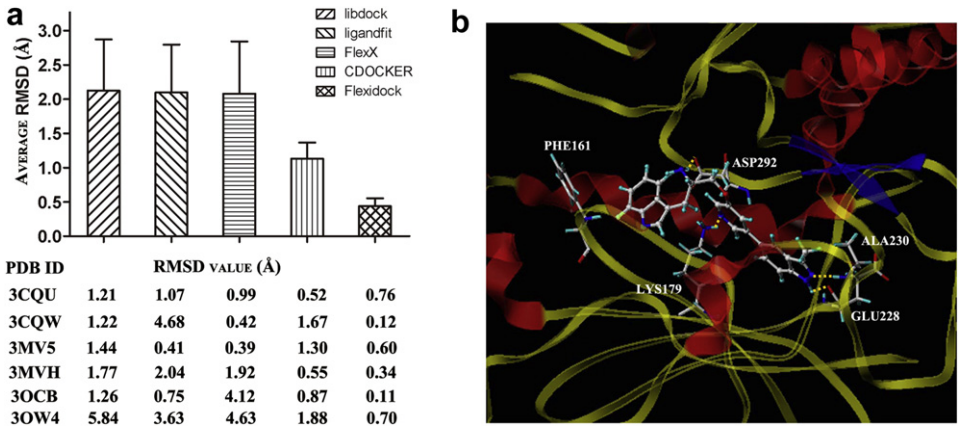

PDB ID	RMSD value (Å)				
3CQU	1.21	1.07	0.99	0.52	0.76
3CQW	1.22	4.68	0.42	1.67	0.12
3MV5	1.44	0.41	0.39	1.30	0.60
3MVH	1.77	2.04	1.92	0.55	0.34
3OCB	1.26	0.75	4.12	0.87	0.11
3OW4	5.84	3.63	4.63	1.88	0.70

Fig. 3. Interaction mode between PKB/Akt1 and ligands proposed by molecular docking. (a) Redock studies on six PKB/Akt1-ligand complex using Libdock, LigandFit, FlexX, CDOCKER and Fleixidock programs; (b) Interaction mode between PKB/Akt1 and compound **1** proposed by FlexiDock, hydrogen bond interaction between ligand and enzyme were highlighted using yellow line. (For interpretation of the references to colour in this figure legend, the reader is referred to the web version of this article.)

including preparation and biological evaluation for their PKB/Akt1 inhibitory activities. **HTS-02143**, **BTB-14740** and **HTS-08006** were purchased from Maybridge chemical (Cornwall, United Kingdom). The synthesis of compounds **75**, **76** and **80** were previously reported [38,39], while the synthesis of compounds **77**–**79** was reported in present study as illustrated in Scheme 1. Prenylchalcones **83** were prepared by Claisen–schmidt condensation of compound **81** with appropriate benzaldehyde **82** in aqueous alcoholic alkali solution. Prenylflavanones **84** were obtained by cyclization of compounds **83** in a solution of sodium acetate in ethanol. Finally, prenylflavones **77**–**79** were obtained by dehydrogenation in the presence of I_2 and pyridine and then demethoxymethylation in catalytic amount of 3N HCl in MeOH/THF (1/1, v/v) using corresponding flavanones **84**, successively.

3.6. Pharmacology

3.6.1. PKB/Akt1 inhibitory activities

PKB/Akt1 inhibitory activities of screened hits were evaluated using HTScan® PKB/Akt1 Kinase Assay Kit (Cell Signaling Technology, Beverly, MA), and compound **H-89**, a known PKB/Akt1 inhibitor [40] was used as positive control. Table 3 lists the biological assay results, indicating that five compounds **75**, **76** and **78**–**80** showed moderate or good PKB/Akt1 inhibitory activities, while **HTS-02143** displayed weak activity. Compounds **79** and **80** showed the best PKB/Akt1 inhibitory activities (IC_{50} of **79** and **80** were 5.4 and 3.9 μM), which were comparable to that of **H-89**. Insight into the observed effects of different substituents of prenylated flavonoids revealed that the 5-OH on A-ring of prenylflavone (**78** is much more potent than **77**), and 3′,4′-$(OH)_2$ on B-ring of prenylflavone (**79**, **80** are potent than **78**) are essential for their PKB/Akt1 inhibitory activities, while the position (C-6 or C-8) of prenyl group at A-ring of prenylflavone has a little effect on the PKB/Akt1 inhibitory activities as exemplified in compounds **79** and **80**. Interestingly, prenylflavones were firstly reported to exhibit significantly PKB/Akt1 inhibitory activities, and would be promising leads for further structural optimization and pharmacological studies.

3.6.2. Cytotoxic activity against cancer cell lines

The cytotoxic activities of compounds **79** and **80** against cancer cell lines (PC3, OVCAR-8 and HL-60) was further investigated, since that PKB/Akt1 is an anti-apoptotic protein kinase and the blockade of its activity leads to cell death. As expected, compounds **79** and **80** showed good anti-proliferative activities against PC3 (**79**: IC_{50} = 14.6 μM; **80**: IC_{50} = 18.6 μM), OVCAR-8 (**79**: IC_{50} = 23.8 μM; **80**: IC_{50} = 16.6 μM) and HL-60 (**79**: IC_{50} = 2.50 μM; **80**: IC_{50} = 3.31 μM) cell lines (Fig. 6a). Apoptosis was assessed using

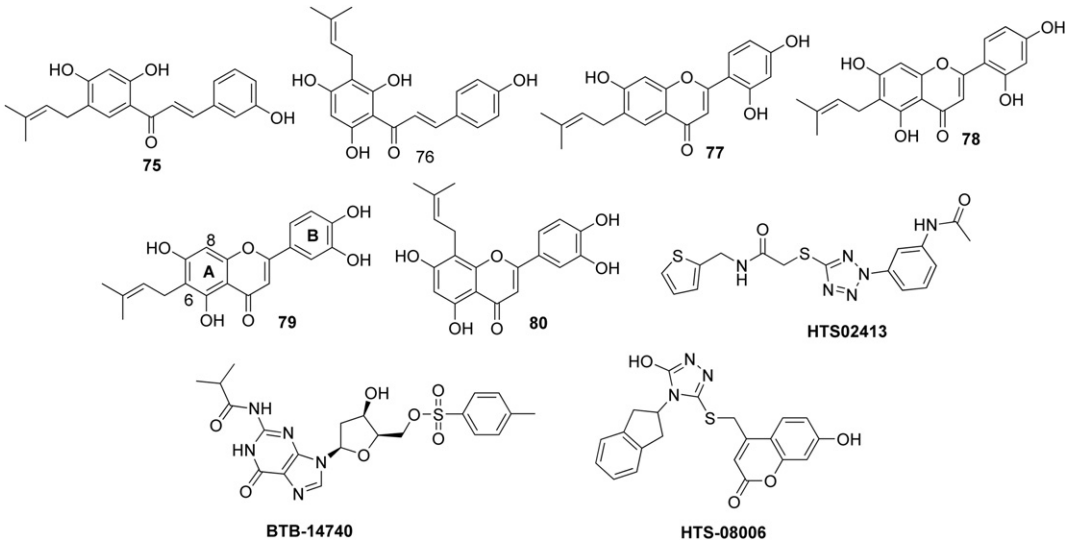

Fig. 4. The 2D structures of preferable screening hits **75**–**80**, **HTS-02143**, **BTB-14740** and **HTS-08006**.

Table 3
The Fit-values, docking energies and PKB/Akt1 inhibitory activities of compounds **75**–**80**, **HTS-02143**, **BTB-14740**, **HTS-08006** and **H-89**.

Compd.	Fit-value[a]	Docking Energy (Kcal/mol)	PKB/Akt1 inhibitory activity IC_{50} (μM)
75	10.2	−2806.3	85.9
76	9.83	−2965.4	143.9
77	7.84	−2828.6	no active
78	8.06	−3319.4	54.48
79	10.8	−3545.0	5.4
80	10.4	−3766.5	3.9
HTS-02143	8.65	−1608.6	>50 (19.6%)
BTB-14740	8.43	−1879.5	no active
HTS-08006	9.63	−2016.9	no active
H-89	/	/	1.8

[a] Fit-value indicates how well the features in the pharmacophore overlap the chemical features in the molecule.

propidium iodide (PI) staining of the sub-G1 cell population, which gains prominence later in apoptosis. Exposure of OVCAR-8 a cells to **79** and **80** for 72 h led to 40.19% and 49.11% cells undergoing apoptosis, respectively (Fig. 6b).

Based on the aforementioned experimental results, we presumed that the inhibition of PKB/Akt pathway contributed to the cytotoxic activities of compounds **79** and **80**. Cell-based assays were conducted to evaluate the effect of compound **79** and **80** on PKB/Akt phosphorylation. Antibodies specific for PKB/Akt phosphorylated at residue Ser-473 were used in immunoblotting experiments. Treatment of OVCAR-8 cells with both of compound **79** and **80** resulted in down-regulation of the phosphorylation of PKB/Akt (Ser-473). Furthermore, the effects on PKB/Akt downstream substrates were next tested. GSK3β is one of the major downstream phosphorylation targets of PKB/Akt. Upon treatment with compound **79** and **80** in OVCAR-8 cells, GSK3β phosphorylation was inhibited, while no significant changes in overall total GSK3β and GAPDH protein levels were observed (Fig. 6c).

4. Conclusion

In this study, we described a rational strategy for identifying novel PKB/Akt1 inhibitors using a pharmacophore-based virtual screen protocol. The best pharmacophore model (Hypo_1) was established using Catalyst/HypoGen program, and showed good statistical parameters in validation process. The Hypo_1 was further employed as a 3D search query to screen our in-house compounds database. Moreover, molecular docking studies were also performed to improve the reliability and accuracy of virtual screening. Then, nine preferable hits were prepared and biological evaluated for their PKB/Akt1 inhibitory activities. Interestingly, five of the hits exhibited moderate or good PKB/Akt1 inhibitory activities, indicating that the pharmacophore-based virtual screening is a rational strategy to discover novel PKB/Akt1 inhibitors. To the best of our knowledge, the 3D alignment and pharmacophoric features of PKB/Akt1 inhibitors and its application in virtual screening were evaluated for the first time. Compounds **79** and **80**, the most potent one, would be good leads to do further structure–activity research

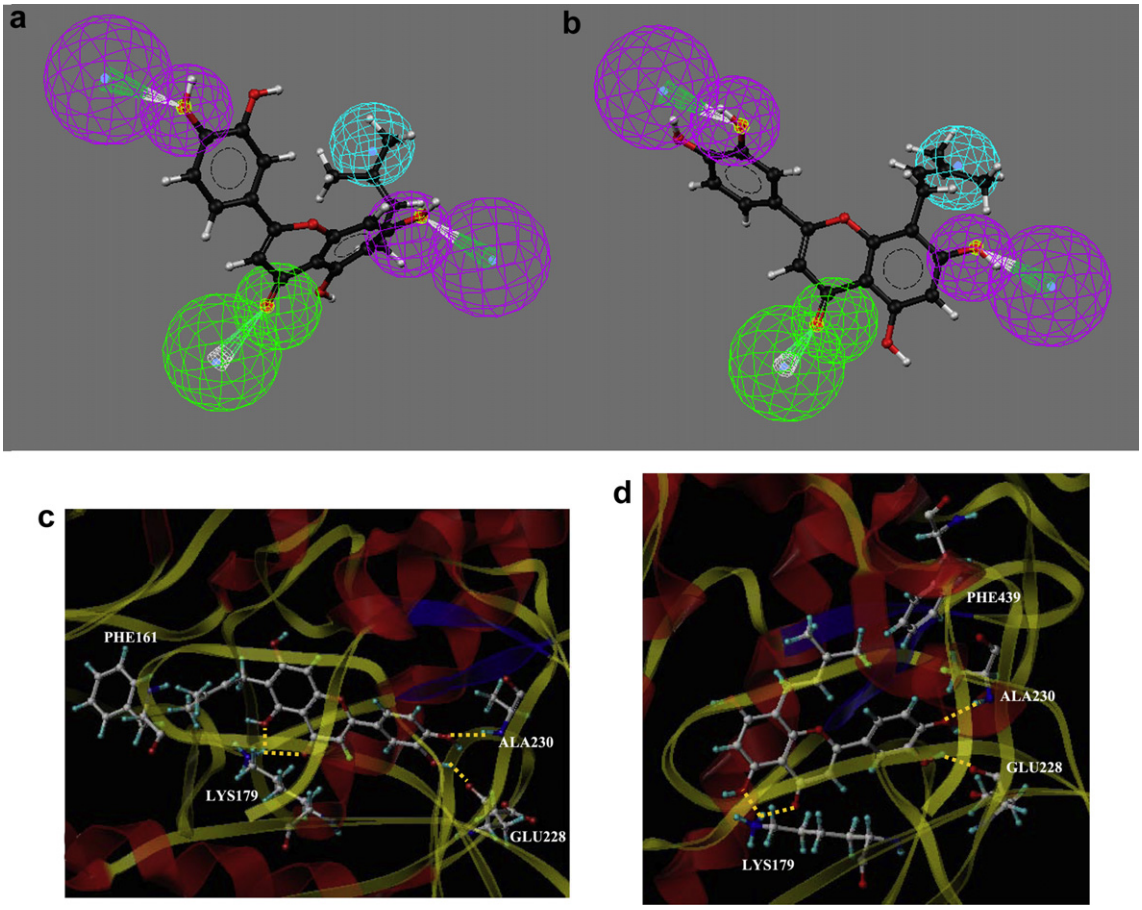

Fig. 5. The virtual evaluated results of preferable hits **79** and **80** by Hypo_1 and molecular docking studies. (a) The compound **79** was aligned to Hypo_1; (b) the compound **80** was aligned to Hypo_1; (c) interaction mode between PKB/Akt1 qand compound **79**, hydrogen bond interaction between ligand and enzyme were highlighted using yellow line; (d) interaction mode between PKB/Akt1 and compound **80**. (For interpretation of the references to colour in this figure legend, the reader is referred to the web version of this article.)

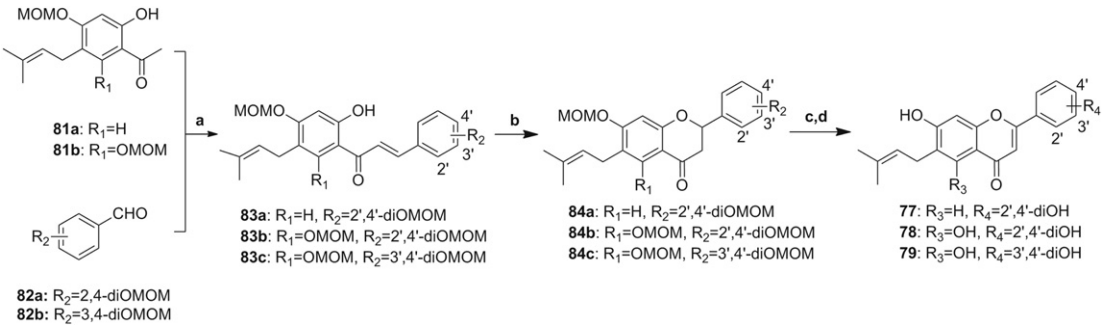

Scheme 1. The synthetic route for compounds **77**–**79**. Reagents and conditions: (a) 10% KOH (H_2O/EtOH = 1/4, v/v); (b): NaOAc, EtOH, reflux; (c) I_2, pyridine, 90 °C; (d): 3N HCl, MeOH/THF, reflux.

to find high potent inhibitors, since that the scaffold was the first time reported to exhibit PKB/Akt1 inhibitory activities.

5. Experimental

5.1. Chemistry

Melting points were obtained on a B-540 Büchi melting point apparatus and are uncorrected. ^{1}H NMR spectra and ^{13}C NMR were recorded on a 400 MHz ^{1}H and 500 MHz ^{1}H (125 MHz ^{13}C) spectromter, respectively. Chemical shifts are expressed as δ values relative to tetramethylsilane (TMS). Mass spectral data were obtained on an Esquire-LC-00075 spectrometer. Elemental analyses were performed on a Flash EA 1112 elemental analyzer. Compounds **75**, **76** and **80** were previously synthesized [32].

5.1.1. General procedure for the synthesis of compounds (*83a*–*c*)

To a cold solution of the acetophenone **81** (1.55 mmol) and appropriate benzaldehyde **82** (1.62 mmol) in H_2O–EtOH (1/4, v/v, 3 mL), KOH (600 mg) in H_2O–EtOH (1/4, v/v, 3 mL) was added with stirring. The resulting mixture was stirred under N_2 atmosphere at room temperature for 36 h. Then, the reaction mixture was poured into ice–water, acidified to pH ~5 with 2 N HCl, and extracted with ethyl acetate. The organic phase was washed with brine, dried over anhydrous Na_2SO_4 and concentrated *in vacuo*. The residue was purified using silica gel column chromatography (petroleum ether:ethyl acetate = 8:1, v/v) to give desired compounds **83**.

*5.1.1.1. 2-Hydroxy-2′,4,4′-trimethoxymethoxy-5-(3,3-dimethylallyl)-chalcone (**83a**).* The product was obtained as a yellow oil (62%). ^{1}H NMR ($CDCl_3$, δ): 1.74 (s, 3H), 1.76 (s, 3H), 3.29 (d, 2H, J = 6.8 Hz), 3.48 (s, 3H), 3.50 (s, 3H), 3.52 (s, 3H), 5.21 (s, 2H), 5.25 (s, 2H), 5.28 (s, 2H), 5.29 (m, 1H), 6.64 (s, 1H), 6.76 (dd, 1H, J = 2.0, 8.0 Hz), 6.87 (d, 1H, J = 2.0 Hz), 7.58 (d, 1H, J = 16.0 Hz), 7.61 (d, 1H, J = 8.0 Hz), 7.62 (s, 1H), 8.17 (d, 1H, J = 16.0 Hz), 13.41 (s, 1H, OH). ESI-MS: m/z $[M + H]^+$ 473.

*5.1.1.2. 2-Hydroxy-2′,4,4′,6-tetramethoxymethoxy-5-(3,3-dimethylallyl)-chalcone (**83b**).* The product was obtained as a yellow oil (52%). ^{1}H NMR ($CDCl_3$, δ): 1.69 (s, 3H,), 1.81 (s, 3H), 3.34 (d, 2H, J = 6.8 Hz), 3.48 (s, 3H), 3.50 (s, 3H), 3.53 (s, 3H), 3.54 (s, 3H),

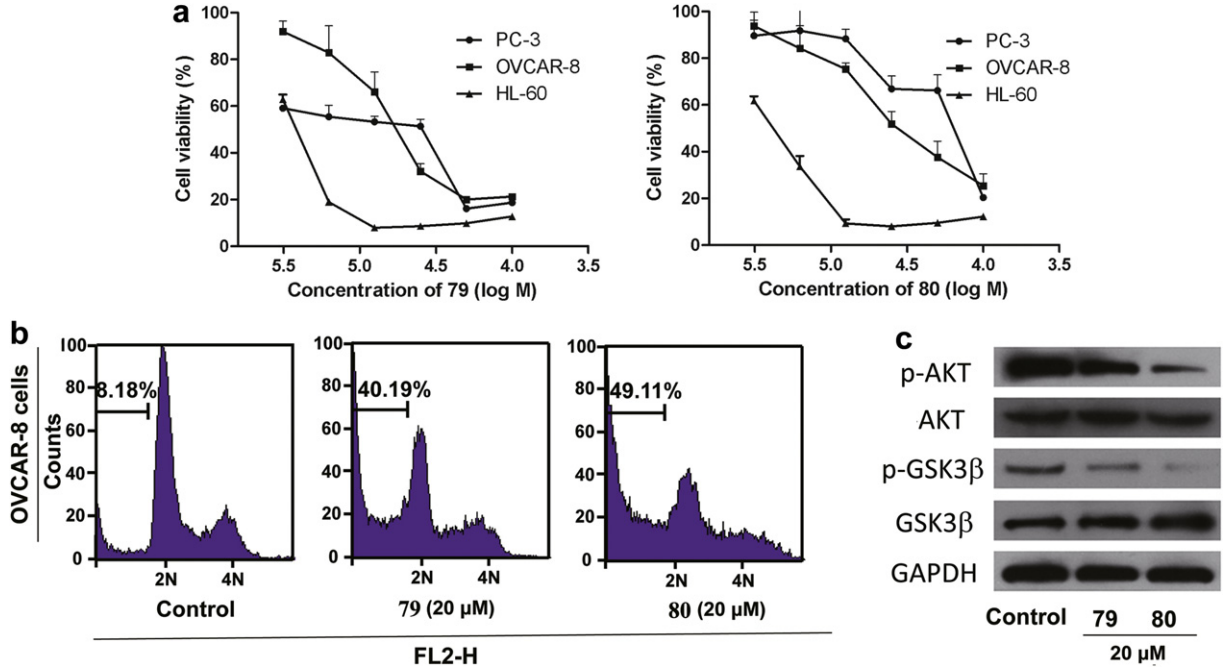

Fig. 6. The cytotoxic activities of **79** and **80** and the preliminary action mechanisms. (a) Cytotoxic activities of **79** and **80** against HL-60, OVCAR-8 and PC-3 cell lines; (b) cell apoptotic index analyses of OVCAR-8 cells exposed to **79** and **80**; (c) treatment with **79** and **80**-caused decrease of PKB/Akt and GSK3β phosphorylation in OVCAR-8 cells.

5.20 (m, 1H), 5.20 (s, 2H), 5.23 (s, 2H), 5.27 (s, 4H), 6.43 (s, 1H,), 6.76 (dd, 1H, J = 2.0, 8.0 Hz), 6.83 (d, 1H, J = 2.0 Hz), 7.63 (d, 1H, J = 8.0 Hz), 7.82 (d, 1H, J = 15.6 Hz), 8.17 (d, 1H, J = 15.6 Hz), 13.88 (s, 1H). ESI-MS: m/z $[M + H]^+$ 533.

*5.1.1.3. 2-Hydroxy-3′,4,4′,6-tetramethoxymethoxy-5-(3,3-dimethylallyl)-chalcone (**83c**).* The product was obtained as a yellow oil (65%). ^{1}H NMR ($CDCl_3$, δ): 1.68 (s, 3H,), 1.76 (s, 3H), 3.32 (d, 2H, J = 6.8 Hz), 3.47 (s, 3H), 3.52 (s, 6H), 3.53 (s, 3H), 5.21 (m, 1H), 5.25 (s, 2H), 5.27 (s, 2H), 5.28 (s, 4H), 6.45 (s, 1H),7.17 (d, 1H, J = 8.8 Hz), 7.21 (dd, 1H, J = 8.8, 1.6 Hz), 7.50 (d, 1H, J = 1.6 Hz), 7.73 (d, 1H, J = 15.6 Hz), 7.84 (d, 1H, J = 15.6 Hz), 13.68 (s, 1H, OH). ESI-MS: m/z $[M + H]^+$ 533.

*5.1.2. General procedure for the synthesis of compounds (**84a–c**)*

A solution of compound **83** (0.8 mmol) and sodium acetate (500 mg) in ethanol (5 mL) containing 3 drops of water was refluxed for 24 h. The mixture was poured into cold water and extracted with ethyl acetate. The organic phase was washed with brine and dried over anhydrous Na_2SO_4. After removing the solvent, the residue was purified using silica gel column chromatography (petroleum ether/ethyl acetate = 4:1) to afford the desired compounds **84**.

*5.1.2.1. 2′,4′,7-Trimethoxymethoxy-6-(3,3-dimethylallyl)-flavanone (**84a**).* The product was obtained as a pale yellow solid (51%), mp.:57–59 °C. ^{1}H NMR ($CDCl_3$, δ): 1.71 (s, 3H), 173 (s, 3H), 2.76 (dd, 1H, J = 3.0, 17.0 Hz), 2.91 (dd, 1H, J = 13.0, 17.0 Hz), 3.28 (d, 2H, J = 7.0 Hz), 3.45 (s, 3H), 3.47 (s, 3H), 3.49 (s, 3H), 5.17 (s, 2H), 5.18 (s, 2H), 5.23 (s, 2H), 5.26 (m, 1H), 5.76 (dd, J = 3.0, 13.0 Hz), 6.69 (s, 1H), 6.79 (dd, 1H, J = 2.0, 8.5 Hz), 6.85 (d, 1H, J = 2.0 Hz), 7.50 (d, 1H, J = 8.5 Hz), 7.71 (s, 1H). ESI-MS: m/z $[M + H]^+$ 473.

*5.1.2.2. 2′,4′,5,7-Tetramethoxymethoxy-6-(3,3-dimethylallyl)-flavanone (**84b**).* The product was obtained as a pale yellow solid (55%). mp.: 83–84 °C. ^{1}H-NMR ($CDCl_3$, δ): 1.68 (s, 3H), 1.79 (s, 3H), 2.76 (dd, 1H, J = 3.0, 16.5 Hz), 2.91 (dd, 1H, J = 12.5, 16.5 Hz), 3.41 (d, 2H, J = 7.0 Hz), 3.46 (s, 3H), 3.48 (s, 3H), 3.50 (s, 3H), 3.63 (s, 3H), 5.19 (s, 2H), 5.20 (s, 2H), 5.21 (s, 2H), 5.22 (m, 1H), 5.23 (s, 2H), 5.72 (dd, J = 3.0, 12.5 Hz), 6.55 (s, 1H), 6.79 (dd, 1H, J = 2.0, 8.5 Hz), 6.86 (d, 1H, J = 2.0 Hz), 7.48 (d, 1H, J = 8.5 Hz). ESI-MS: m/z $[M + H]^+$ 533.

*5.1.2.3. 3′,4′,5,7-Tetramethoxymethoxy-6-(3,3-dimethylallyl)-flavanone (**84c**).* The product was obtained as a pale yellow syrup (45%). ^{1}H NMR ($CDCl_3$, δ): 1.66 (s, 3H), 1.77 (s, 3H), 2.81 (dd, 1H, J = 2.8, 17.2 Hz), 2.30 (dd, 1H, J = 13.2, 17.2 Hz), 3.32 (d, 2H, J = 6.8 Hz), 3.47 (s, 3H), 3.52 (s, 3H), 3.53 (s, 6H), 5.21 (m, 1H), 5.23 (s, 2H), 5.25 (s, 4H), 5.26 (s, 2H), 5.33 (dd, 1H, J = 2.8 Hz, 13.2 Hz), 6.56 (s, 1H), 7.04 (dd, 1H, J = 2.0, 8.0 Hz), 7.19 (d, 1H, J = 8.0 Hz), 7.31 (d, 1H, J = 2.0 Hz). ESI-MS: m/z $[M + H]^+$ 533.

*5.1.3. General procedure for the synthesis of compounds **77–79***

A stirred solution of corresponding **84** (0.3 mmol) and iodine (0.3 mmol) in dry pyridine (4 mL) was heated to 90 °C for 6 h. The mixture was then poured into cold water, acidified to pH ~ 6 with 2 N HCl, then extracted with ethyl acetate. The organic phase was washed with saturated sodium thiosulfate and water, successively. Then the organic layer was washed with brine and dried over anhydrous Na_2SO_4 and concentrated. The residue was dissolved in methanol/THF (1/1, v/v, 5 mL) without purification, and 3N HCl (0.5 mL) was added. The mixture was stirred at 50 °C for 6 h. After cooling to room temperature, the reaction mixture was poured into cold water and extracted with ethyl acetate. The organic phase was washed with brine, dried over anhydrous Na_2SO_4. After removal of the solvent, the residue was purified using silica gel column chromatography (petroleum ether: ethyl acetate = 2:1, v/v) to give desired compounds **77–79**.

*5.1.3.1. 2′,4′,7-Trihydroxy-6-(3,3-dimethylallyl)-flavone (**77**).* Pale yellow solid (68%), mp: 192–194 °C; ^{1}H NMR (Acetone-d6, δ): 1.74 (s, 3H), 1.76 (s, 3H), 3.41 (d, 2H, J = 7.5 Hz), 5.40 (m, 1H), 6.55 (dd, 1H, J = 2.0, 8.5 Hz), 6.61 (d, 1H, J = 2.5 Hz), 7.02 (s, 1H), 7.08 (s, 1H), 7.78 (d, 1H, J = 8.5 Hz), 7.83 (s, 1H), 8.86 (s, 1H, OH), 9.40 (s,1H, OH), 9.58 (s, 1H, OH). ^{13}C NMR (Acetone-d6, δ): 181.2, 166.5, 162.3, 160.1, 157.8, 136.2, 131.5, 130.1, 126.5, 124.6, 123.9, 118.2, 112.1, 109.7, 107.6, 104.3, 102.1, 27.6, 22.2, 18.1. ESI-MS: m/z $[M + H]^+$ 339. Anal. calcd. for $C_{20}H_{18}O_5$: C, 70.99; H, 5.36; Found C, 70.87; H, 5.49.

*5.1.3.2. 2′,4′,5,7-Tetrahydroxy-6-(3,3-dimethylallyl)-flavone (**78**).* Pale yellow solid (41%), mp: >240 °C (des.); ^{1}H NMR (Acetone-d6, δ): 1.60 (s, 3H), 1.73 (s, 3H), 3.30 (d, 2H, J = 7.2 Hz), 5.23 (m, 1H), 6.49 (dd, 1H, J = 2.0, 8.0 Hz), 6.51 (s, 1H), 6.55 (d, 2H, J = 2.0 Hz), 7.00 (s, 1H), 7.75 (d, 1H, J = 8.0), 8.96 (s, 1H, OH), 9.45 (s,1H, OH), 9.50 (s, 1H, OH), 13.35 (s, 1H, OH). ^{13}C NMR (Acetone-d6, δ): 182.1, 163.6, 162.3, 161.7, 159.2, 158.9, 156.1, 130.8, 129.6, 123.3, 110.6, 109.7, 108.7, 106.8, 105.9, 103.2, 94.6, 25.5, 21.2, 17.8. ESI-MS: m/z $[M + H]^+$ 355. Anal. calcd. for $C_{20}H_{18}O_6$: C, 67.79; H, 5.12; Found C, 67.66; H, 5.30.

*5.1.3.3. 3′,4′,5,7-Tetrahydroxy-6-(3,3-dimethylallyl)-flavone (**79**).* Pale yellow solid (35%), mp: >210 °C (des.); ^{1}H NMR (Acetone-d6, δ): 1.65 (s, 3H), 1.78 (s, 3H), 3.35 (d, 2H, J = 7.2 Hz), 5.28 (m, 1H), 6.56 (s, 1H), 6.60 (s, 1H), 6.99 (d, 1H, J = 8.5 Hz), 7.44 (dd, 1H, J = 2.0, 8.5 Hz), 7.48 (d, 1H, J = 2.0 Hz), 8.98 (s, 1H, OH), 9.47 (s,1H, OH), 9.52 (s, 1H, OH), 13.28 (s, 1H, OH). ^{13}C NMR (Acetone-d6, δ): 183.8, 165.2, 162.8, 161.3, 157.5 150.1, 147.4, 131.8, 124.6, 123.7, 120.0, 116.5, 114.3, 112.2, 105.4, 104.5, 94.3, 25.7, 22.1, 18.0. ESI-MS: m/z $[M + H]^+$ 355. Anal. calcd. for $C_{20}H_{18}O_6$: C, 67.79; H, 5.12; Found C, 67.62; H, 4.97.

5.2. Pharmacological assay

5.2.1. PKB/Akt1 assay

In vitro kinase assays were carried out using HTScan® PKB/Akt1 Kinase Assay Kit (Cell Signaling Technology, Beverly, MA). Active recombinant Akt1 kinase (GST-fusion protein, 4 ng) in 8 μL of 2.5 × kinase buffer [62.5 mM Tris–HCl (pH 7.5), 25 mM $MgCl_2$, 12.5 mM β-glycerophosphate, 0.25 mM Na_3VO_4, 5 mM dithiothreitol (DTT)], was mixed with 2 μL of dimethyl sulfoxide (DMSO) vehicle or each of the compound (indicated concentrations), incubated at room temperature for 5 min and 10 μL of ATP/substrate cocktail (20 mM ATP, 3 mM eNOS served as substrate) was added. After incubation at room temperature for 30 min, add 20 μL of 50 mM ethylenediaminetetraacetic acid (EDTA) (pH 8.0) and terminate the reaction. Then, PKB/Akt1 kinase activity was analyzed according to the manufacturer's instructions.

5.2.2. Cytotoxic activity assay

The cytotoxic activity of the tested compounds in PC3, OVCAR-8 and HL-60 cells was measured using the MTT (3-(4,5-Dimethylthiazol-2-yl)-2,5-diphenyltetrazolium bromide, a tetrazole) method. Cells were seeded in 96-well microtiter plates (at a density of 4000 cells per well) for overnight attachment and exposed to each of the compound (1.0 ~ 100.0 μM) for 72 h. The MTT solution (5.0 mg/mL in RPIM 1640 medium; Sigma-Aldrich) was added (20.0 μl/well), and plates were incubated for a further 4 h at 37 °C. The purple formazan crystals were dissolved in 100.0 μL of DMSO. After 5 min, the plates were read on an automated microplate spectrophotometer (Bio-Tek Instruments, Winooski, VT) at 570 nm. Assays were

performed in triplicate on three independent experiments. The concentration of drug inhibiting 50% of cells (IC_{50}) was calculated using the software of dose–effect analysis with microcomputers.

5.2.3. Apoptosis assay

To analysis apoptosis, OVCAR-8 cells (5 × 104 cells/ml, 5 mL) were cultured in 25 cm^2 flasks and treated with vehicle to test compounds (20 μM). After 48 h of treatments, cells were harvested and quickly washed twice with ice-cold PBS. Detection of apoptosis by FACSCalibur flow cytometer (Becton Dickinson, Lincoln Park, NJ) was performed using the Annexin V-FITC/Propidium iodide (PI) apoptosis detection kit (BioVision, Mountain View, CA).

5.2.4. Western blotting assay

OVCAR-8 cells were harvested, washed with ice-cold 1 × phosphate-buffered saline (PBS), and lysed in immunoprecipitation assay buffer [150 mM NaCl, 50 mMTris, 2 mM ethyleneglycol-bis(b-aminoethylether), 2 mM EDTA, 25 mM NaF, 25 mM b-glycerophosphate, 0.2% TritonX-100, 0.3% Nonidet P-40, and 0.1 mM phenylmethylsulfonyl fluoride]. Cellular debris were pelleted by centrifugation at 13,000 rpm for 30 min at 4 °C. The concentrations of the total lysate protein were measured using a standard Bradford assay (Bio-Rad, San Diego, CA). For Western blot analysis, 40 ∼ 80 μg of protein from the total cell lysate was electrophoresed by SDS–PAGE. The proteins were then transferred to nitrocellulose membrane (Pierce Chemical) and probed with primary antibodies followed by horseradish peroxidase-labeled secondary antibodies. Proteins were visualized using enhanced chemiluminescence (Pierce Chemical).

Acknowledgments

This study was financially supported by the China Postdoctoral Science Foundation (NO. 20090460103), National Natural Science Foundation of China (No. 201003734) and National Key Tech Project for Major Creation of New drugs (NO. 2009ZX09501-003).

References

[1] J. Brognard, A.S. Clark, Y. Ni, P.A. Dennis, Cancer Res. 61 (2001) 3986–3997.
[2] J.Q. Cheng, B. Ruggeri, W.M. Klein, G. Sonoda, D.A. Altomare, D.K. Watson, J.R. Testa, Proc. Natl. Acad. Sci. U.S.A 93 (1996) 3636–3641.
[3] D. Haas-Kogan, N. Shalev, M. Wong, G. Mills, G. Yount, D. Stokoe, Curr. Biol. 8 (1998) 1195–1198.
[4] S.P. Staal, Proc. Natl. Acad. Sci. U.S.A 84 (1987) 5034–5037.
[5] E. Fayard, L. Tintignac, A. Baudry, B. Hemmings, J. Cell. Sci. 118 (2005) 5675–5678.
[6] S. Masure, B. Haefner, J.J. Wesselink, E. Hoefnagel, E. Mortier, P. Verhasselt, A. Tuytelaars, R. Gordon, A. Richardson, Eur. J. Biochem. 265 (1999) 353–360.
[7] R.T. Joseph, B. Alfonso, Proc. Natl. Acad. Sci. U.S.A 98 (2001) 10983–10985.
[8] E. Oki, H. Baba, E. Tokunaga, T. Nakamura, N. Ueda, M. Futatsugi, K. Mashino, M. Yamamoto, M. Ikebe, Y. Kakeji, Y. Maehara, Int. J. Cancer 117 (2005) 376–380.
[9] C. Sourbier, V. Lindner, H. Lang, A. Agouni, E. Schordan, S. Danilin, S. Rothhut, D. Jacqmin, J. Helwig, T. Massfelder, Cancer Res. 66 (2006) 5130–5142.
[10] E. Tokunaga, A. Kataoka, Y. Kimura, E. Oki, K. Mashino, K. Nishida, T. Koga, M. Morita, Y. Kakeji, H. Baba, S. Ohno, Y. Maehar, Eur. J. Cancer 42 (2006) 629–635.
[11] D. Mahadevan, G. Powis, E.A. Mash, B. George, V.M. Gokhale, S. Zhang, K. Shakalya, L. Du-Cuny, M. Berggren, M.A. Ali, U. Jana, N. Ihle, S. Moses, C. Franklin, S. Narayan, N. Shirahatti, E.J. Meuillet, Mol. Cancer Ther. 7 (2008) 2621–2632.
[12] C.W. Lindsley, S.F. Barnett, M. Yaroschak, M.T. Bilodeau, M.E. Layton, Curr. Top. Med. Chem. 7 (2007) 1349–1363.
[13] C.W. Lindsley, Z. Zhao, W.H. Leister, R.G. Robinson, S.F. Barnett, D. Defeo-Jones, R.E. Jones, G.D. Hartman, J.R. Huff, H.E. Huber, M.E. Duggan, Bioorg. Med. Chem. Lett. 15 (2005) 761–764.
[14] Q. Li, T. Li, G. Zhu, J. Gong, A. Claibone, C. Dalton, Y. Luo, E.F. Johnson, Y. Shi, X. Liu, V. Klinghofer, J.L. Bauch, K.C. Marsh, J.J. Bousk, S. Arries, R. de Jong, T. Oltersdorf, V.S. Stoll, C.G. Jakob, S.H. Rosenberg, V.L. Giranda, Bioorg. Med. Chem. Lett. 16 (2006) 1679–1685.
[15] G. Zhu, J. Gong, A. Claiborne, K.W. Woods, V.B. Gandhi, S. Thomas, Y. Luo, X. Liu, Y. Shi, R. Guan, S.R. Magnone, V. Klinghofer, E.F. Johnson, J. Bouska, A. Shoemaker, A. Oleksijew, V.S. Stoll, R. de Jong, T. Oltersdorf, Q. Li, S.H. Rosenberga, V.L. Giranda, Bioorg. Med. Chem. Lett. 16 (2006) 3150–3155.
[16] K.W. Woods, J.P. Fischer, A. Claiborne, T. Li, S.A. Thomas, G. Zhu, R.B. Diebold, X. Liu, Y. Shi, V. Klinghofer, E.K. Han, R. Guan, S.R. Magnone, E.F. Johnson, J.J. Bouska, A.M. Olson, R. de Jong, T. Oltersdorf, Y. Luo, S.H. Rosenberg, V.L. Giranda, Q. Li, Bioorg. Med. Chem. Lett. 14 (2006) 6832–6848.
[17] G. Zhu, J. Gong, V.B. Gandhi, K. Woods, Y. Luo, X. Liu, R. Guan, V. Klinghofer, E.F. Johnson, V.S. Stoll, M. Mamo, Q. Li, S.H. Rosenberg, V.L. Giranda, Bioorg. Med. Chem. Lett. 15 (2007) 2441–2452.
[18] G. Zhu, V.B. Gandhi, R. de Jong, Y. Luo, X. Liu, Y. Shi, R. Guan, S.R. Magnone, V. Klinghofer, E.F. Johnson, J. Bouska, A. Shoemaker, A. Oleksijew, K. Jarvis, C. Park, R. de Jong, T. Oltersdorf, Q. Li, S.H. Rosenberg, V.L. Giranda., Bioorg. Med. Chem. Lett. 16 (2006) 3424–3429.
[19] O. Dror, A. Shulman-Peleg, R. Nussinov, H.L. Wolfson, Curr. Med. Chem. 11 (2004) 71–90.
[20] S. Vadivelan, B.N. Sinha, G. Rambabu, K. Boppana, S.A. Jagarlapudi, J. Mol. Graph. Model. 26 (2008) 935–946.
[21] A. Rinaldi, EMBO Rep. 9 (2008) 1073–1077.
[22] L. Di, E.H. Kerns, Curr. Opin. Drug Discov. Devel. 8 (2005) 495–504.
[23] S.L. Dixon, Chem. Biol. Drug Des. 67 (2006) 370–372.
[24] T.A. Esbenshade, G.B. Fox, K.M. Krueger, T.R. Miller, C.H. Kang, L.I. Denny, D.G. Witte, B.B. Yao, L. Pan, J. Wetter, K. Marsh, Y.L. Bennani, M.D. Cowart, J.P. Sullivan, A.A. Hancock, J. Pharmacol. Exp. Ther. 313 (2005) 165–175.
[25] H.J. Boehm, M. Boehringer, D. Bur, H. Gmuender, W. Huber, W. Klaus, D. Kostrewa, H. Kuehne, T. Luebbers, N. Meunier-Keller, F. Mueller, J. Med. Chem. 43 (2000) 2664–2674.
[26] H. Yu, Z. Wang, L. Zhang, J. Zhang, Q. Huang, Bioorg. Med. Chem. Lett. 17 (2007) 2126–2133.
[27] G. Zhu, V.B. Gandhi, J. Gong, S. Thomas, K.W. Woods, X. Song, T. Li, R.B. Diebold, Y. Luo, X. Liu, R. Guan, V. Klinghofer, E.F. Johnson, J. Bouska, A. Olson, K.C. Marsh, V.S. Stoll, M. Mamo, J. Polakowski, T.J. Campbell, R.L. Martin, G.A. Gintant, T.D. Penning, Q. Li, S.H. Rosenberg, V.L. Giranda, J. Med. Chem. 50 (2007) 2990–3003.
[28] B.R. Brooks, R.E. Brucolleri, B.D. Olafson, D.J. States, S.S., M. Karplus, J. Comput. Chem. 4 (1983) 187–214.
[29] A. Smellie, S.D. Kahn, S.L. Teig, J. Chem. Inf. Comp. Sci. 35 (1995) 285–294.
[30] A.K. Debnath, J. Med. Chem. 45 (2002) 41–53.
[31] W.M. Kazmierski, W. Andrews, E. Furfine, A. Spaltenstein, L. Wright, Bioorg. Med. Chem. Lett. 14 (2004) 5689–5692.
[32] T. Fawcett, Pattern. Recogn. Lett. 27 (2006) 861–874.
[33] Sybyl6.9 (2002), Molecular Modelling System, Tripos Associates: St. Louis, MO, USA.
[34] M. Rarey, B. Kramer, T. Lengauer, G. Klebe, J. Mol. Biol. 261 (1996) 470–489.
[35] C.M. Venkatachalam, X. Jiang, T. Oldfield, M. Waldman, J. Mol. Graphics Model. 21 (2003) 289–307.
[36] G. Wu, D.H. Robertson, C.L. Brooks 3rd, M. Vieth, J. Comput. Chem. 24 (2003) 1549–1562.
[37] S.N. Rao, M.S. Head, A. Kulkarni, J.M. LaLonde, J. Chem. Inf. Model. 47 (2007) 2159–2171.
[38] X. Dong, J. Chen, C. Jiang, T. Liu, Y. Hu, Arch. Pharm. 342 (2009) 428–432.
[39] X. Dong, L. Qi, C. Jiang, J. Chen, E. Wei, Y. Hu, Bioorg. Med. Chem. Lett. 19 (2009) 3196–3198.
[40] C.K. Chandra, M. Vincent, AKT crystal structure and AKT-specific inhibitors, Oncogene 24 (2005) 7493–7501.